Regular Article

ANALYTICAL AND BIOANALYTICAL CHEMISTRY RESEARCH

Published by the
Iranian Chemical Society

***Anal. Bioanal. Chem. Res.**, Vol. 8, No. 2, 113-128, December 2020.*

Evaluation of Corrosion Inhibition and Adsorption Behavior of 7-Isopropyl-4-methyl-4,5,6,7-tetrahydrobenzoisoxazole against Carbon Steel Corrosion in 1 M HCl. Experimental and Computational Investigations

Abdeslam Ansari[a,*], Zouhair Lakbaibi[b,*], Mohamed Znini[b], Mounir Manssouri[b] and Amal Laghchimi[b]

[a]*Moulay Ismail University of Meknes, Laboratory of chemistry physics of Materials, Faculty of Sciences and Techniques, P.B 509, 52000, Errachidia, Morocco*

[b]*Moulay Ismail University of Meknes, Laboratory of Natural Substances & Synthesis and Molecular Dynamics, Faculty of Sciences and Techniques, P.B 509, 52000, Errachidia, Morocco*

(Received 2 June 2020 Accepted 13 October 2020)

The corrosion inhibition capabilities of menthone, discovered in 2014 by our team, encouraged us to prepare again a new derivative of menthone called 7-isopropyl-4-methyl-4,5,6,7-tetrahydrobenzoisoxazole (MD). This compound was characterized by FT-IR, ^{1}H NMR and ^{13}C NMR techniques. Then, the evaluation of corrosion inhibition and adsorption behavior of MD onto carbon steel was carried out in 1 M HCl using the weight loss analysis and electrochemical methods such as potentiodynamic polarization (PDP), and electrochemical impedance spectroscopy. The inhibition efficiency was increased by the increase of both the dose of MD (0.72 to 5.65 mM) and the temperature of the medium (298 to 323 K). The thermodynamic kinetic parameters showed that the adsorption of MD on the carbon steel surface follows the Langmuir adsorption isotherm. Furthermore, PDP measurements exhibited that the studied MD inhibitor performs as a mixed-type inhibitor. Finally, the density functional theory, molecular electrostatic potential and Monte Carlo studies were performed to gain an insight about adsorption mechanism, indicating that the MD inhibitor can effectively limit corrosion onto the carbon steel surface. Based on the results, we have concluded that the synthesized MD can be used as an efficient inhibitor to stop carbon steel surface corrosion.

Keywords: Menthone derivative, Corrosion inhibitor, Density functional theory, Monte Carlo Simulation

INTRODUCTION

Carbon steel is one of the major building materials that are widely used in industry [1,2]. In acidic medium, this metal is attacked by the aggressiveness of corrosive environments. To limit its potential corrosion, many organic compounds containing hetero-atoms, lone pair electrons, double/triple bonds, aromatic ring, or all, have proven to be among the most effective organic corrosion inhibitors. Several studies in this field reveal that these organic inhibitors can adhere to the surfaces of metals *via* adsorption of polar functional groups including heteroatoms (N, P, O and S) an the π-electrons of functional groups and aromatic rings that form a protective surface [3,4]. Typically, this metal/inhibitor adsorption depends on the nature of the electrode surface, electrochemical potentials at the metal/solution interface as well as the structure and electronic properties of the inhibitor [5,6]. In this regard, numerous studies have revealed that monoterpenoid ketones possess corrosion-inhibiting properties in the acidic medium [7-9]. For instance, we reported previously that menthone is an efficient corrosion inhibitor for steel in acidic media [10]. In continuation of our work and to improve the inhibition efficiencies of menthone we have synthesized the

*Corresponding author. E-mail: ansdesa2@yahoo.fr

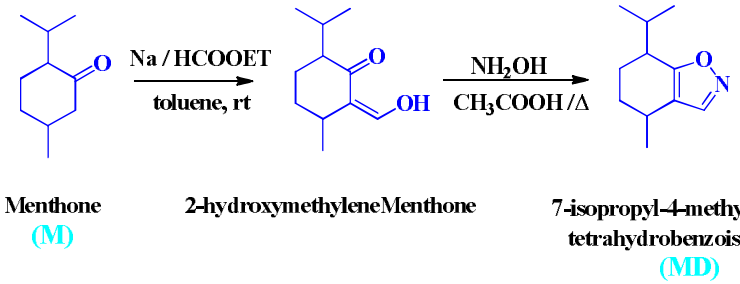

Scheme 1. Synthesis of 7-isopropyl-4-methyl-4,5,6,7-tetrahydrobenzoisoxazole (MD)

menthone derivative comprising of some electron-rich active sites in the form of heteroatoms (oxygen and nitrogen) and π-electrons. In addition, computational approaches have been also widely used to a deep understanding of the adsorption mechanism between the metal surface and inhibitor, elucidating the chemical and physical properties of structures and sometimes proving the adsorption behavior of inhibitor compound towards the metal surface [11,12]. Our study here contains four parts; i) synthesis of new menthone derivative, namely, 7-isopropyl-4-methyl-4,5,6,7-tetrahydrobenzoisoxazole (MD), and its characterization using FT-IR, ^{1}H NMR and ^{13}C NMR techniques, ii) testing the corrosion inhibition of MD using the monitoring techniques such as low weight measurements and electrochemical methods, and iii) using the modeling approaches such as the density functional theory (DFT), molecular electrostatic potential (MEPS) and Monte Carlo (MC) to evaluate the corrosion inhibition and adsorption behavior of the MD towards the iron surface (110) (the main constituent of CS) in 1 M HCl as corrosive solution medium. The corrosion inhibition process is carried out in acidic solution that consequently leads to protonation of inhibitors with both lone pair of electrons and possibly the increase of nucleophilic sites of carbon atoms. To verify this, the calculation results of non-protonated forms will be discussed, and then compared to those of the protonated forms.

EXPERIMENTAL

Synthesis of MD

All chemical reagents designed for this synthesis were of analytical grades and obtained from Aldrich Chemical Co. The preparation of the 2-hydroxymethylenementhone intermediate was required for the synthesis of 7-isopropyl-4-methyl-4,5,6,7-tetrahydrobenzoisoxazole (MD) started with the formylation of menthone (M) previously reported in our publication [13] (Scheme 1). To do so, to a solution of hydroxylamine (NH_2OH) (0.08 mol) and 40.0 ml of toluene as a solvent, 2-hydroxymethylenementhone (0.04 mol) was added. The reaction mixture was then refluxed for 4 h. After rearward filtration, the solvent was removed under reduced pressure. The residue was purified by column chromatography affording the corresponding product 7-isopropyl-4-methyl-4,5,6,7-tetrahydrobenzo-isoxazole (MD) in 75% yield (Scheme 1). The MD product was characterized by deducing NMR1H, NMR13C and infrared data (Fig. 1 and Table 1)

Preparation of CS Samples, Corrosive Solutions, and Inhibitors

Corrosion tests were performed on the CS samples with dimension of 2×2×2 cm; the CS metal presents the subsequent composition with mass percentages (%): P 0.09, Si 0.38, Al 0.01, Mn 0.05, C 0.21, S 0.05 and Fe 99.21. Before each corrosion test, the MS samples were mechanically grazed with sequential grades emery papers (400, 600 and 1200 grit), and ensuing rinsed and degreased with distilled water and acetone, respectively, then dried and weighed. The corrosive acid solution (a molar hydrochloric acid (1 M of HCl)) was prepared from the concentrated commercial acid of HCl (37%) by dilution with distilled water. For the three corrosion monitoring techniques (WL, EIS and PDP), we worked in the different concentrations of inhibitor (MD) as follows: 0.7, 1.4, 2.8 and 5.58 mM.

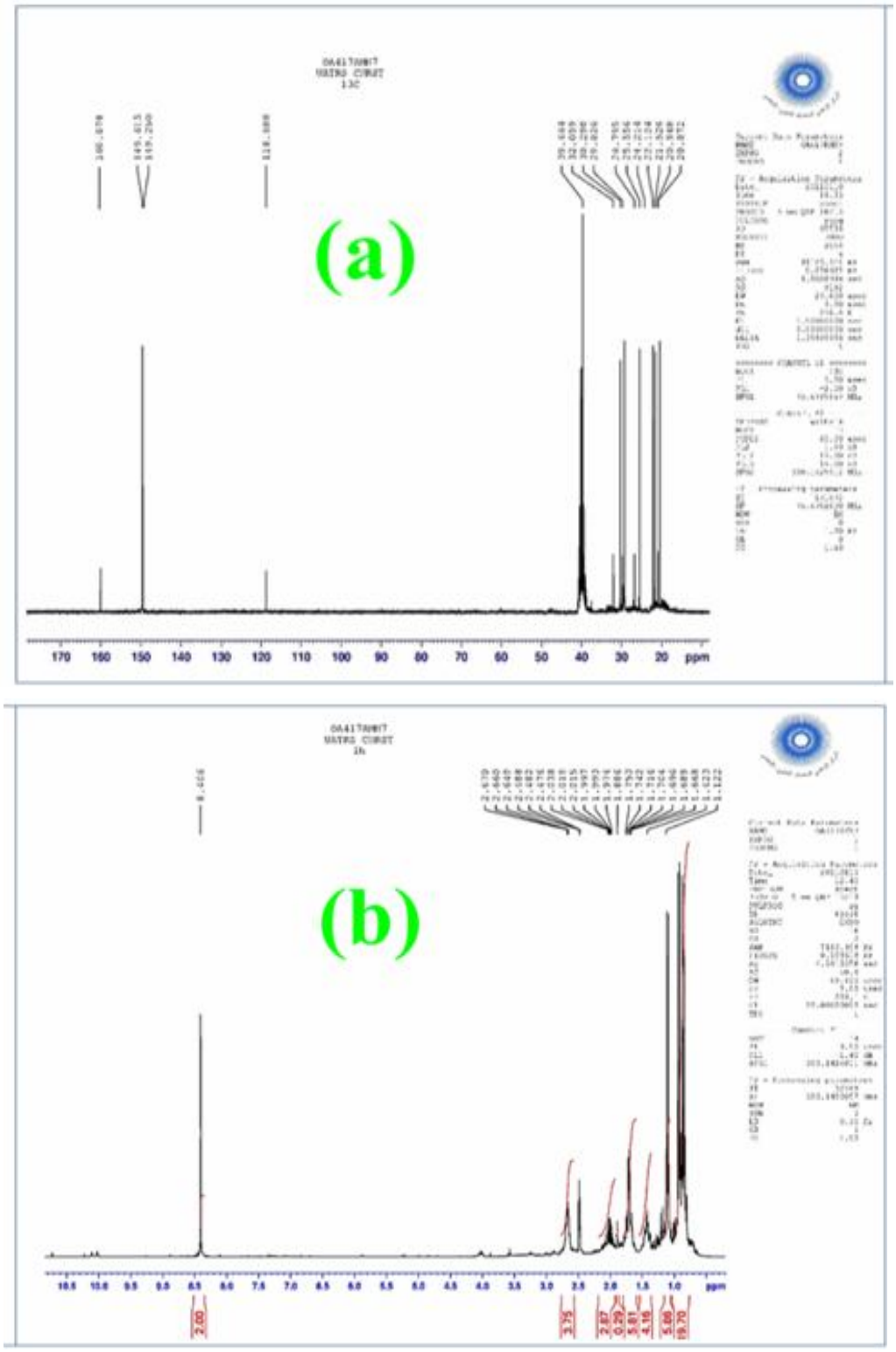

Fig. 1. ^{1}H NMR (a) and ^{13}C NMR (b) spectra of MD.

Table 1. Spectral Characterization Data of MD

IR data	^{1}H NMR data	^{13}C NMR data
$\nu_{=C-H}$ 2959; ν_{C-H} 2932.	7.36 (S, 1H); 2.78 (m, 1H); 2.14	18.73 (CH_3); 20.19 (CH_3);
ν_{C-H} 2872; $\nu_{C=N}$ 1625; $\nu_{C=C}$ 1458;	(m, 2H); 1.50 (m, 2H); 0.9 (d,	22.3 (CH_3); 26.1 (CH); 29.65
ν_{C-O} 1227.	3H);1.22 (d, 3H); 1.04 (d, 3H);	(CH_2); 30.8 (CH); 38.7 (CH);
	0.68 (d, 3H)	122 (CH); 132 (C); 144 (C).

Corrosion Monitoring Techniques

Weight loss (WL) measurements. The prepared CS samples were weighed, and then immersed in 1 M HCl with and without different concentrations from 0.7 to 5.6 mM of MD under different temperatures of 298 to 328 K after an exposure time of 6 h [14]. Inhibitory efficiency (*IE%*) is determined based on the CS corrosion rates *W* (mg cm^{-2} h^{-1}) according to the subsequent relationship (Eqs. (1), (2)) [15]:

$$W = \frac{m_b - m_a}{S.t} \quad (1)$$

where m_b and m_a (mg) are the CS sample weights before and after immersion in the tested solution. *S* is the area of the CS sample (cm^2) and *t* is the exposure time (h),

$$IE\% = \frac{W_{HCl} - W_{inh}}{W_{HCl}} \times 100 \quad (2)$$

where W_{HCl} and W_{inh} are the MS corrosion rates in both uninhibited and inhibited solutions, respectively. The extent of the surface coverage (θ) is defined as follows (Eq. (3)) [16]:

$$\theta = \frac{IE\%}{100} \quad (3)$$

Electrochemical (PDP and EIS) measurements. Before realizing each electrochemical corrosion test, the studied CS was immersed in the test solution for 30 min at the open circuit potential (E_{OCP}) to find a steady-state. Both PDP and EIS tests were performed utilizing an assembly of the electrochemical cell containing three electrodes: a disc cut form of CS as a working electrode (1 cm^2), a saturated calomel electrode (Ag/AgCl) as a reference electrode and a platinum electrode as against electrode. All electrochemical measurements were carried out using a potentiostat/ galvanostat (Model 263A) and the electrochemical parameters values were determined using the Volta Master 4 software. We note that all potentials measurements in this study were obtained concerning the potential value of the reference electrode.

The PDP tests are achieved in 1 M HCl (without MD) and in different concentrations of MD concentrations (0.7 to 5.6 mM) at the temperature range of 298-328 K, simultaneously. Furthermore, the cathodic and anodic curves are plotted by varying the electrode potential between -800 and +800 mV versus reference electrode at open circuit potential with a scan rate of 0.5 mV s^{-1}. Inhibitory efficiency (*IE%*) is determined based on the current corrosion *i* of CS at the above conditions according to following equation (Eq. (4)):

$$IE\% = \frac{i_{HCl} - i_{inh}}{i_{HCl}} \times 100 \quad (4)$$

where i_{HCl} and i_{inh} are the corrosion current densities without and with inhibitor, respectively. Total charge transfer resistances $R_{t(HCl)}$ (without MD) and $R_{t(inh)}$ (with MD) were calculated from Nyquist plots by measuring the impedance difference at low and high frequencies. We maintained the above experiment conditions, and then we performed the EIS tests in the frequency series varying from 100 kHz to 10 MHz at open circuit potential with a signal amplitude of 10 mV. The inhibitory efficiency (*IE%*) is designed

according to Eq. (5).

$$IE\% = \frac{R_{t(inh)} - R_{t(HCl)}}{R_{t(inh)}} \times 100 \quad (5)$$

The capacity of the double layer (C_{dl}) is determined as follows (Eq. (6)) [17]:

$$C_{dl} = \frac{1}{2\pi f_{max} R_t} \quad (6)$$

f_{max} is the frequency for which the imaginary part of the impedance is maximum.

Theoretical Procedures

DFT and MESP calculations. The optimized geometries of both MD (neutral form) and MDH+ (protonated form) were performed using DFT method [18] embedded in Gaussian 09 software [19] in the scheme of B3LYP [20] with the 6-31G++(d,p) [21]. Then, we calculated the following global quantum descriptors for the target structures: energy of HOMO (highest occupied molecular orbital) and LUMO (lowest unoccupied molecular orbital), the electronegativity χ ($\chi = -(E_{HOMO} + E_{LUMO})/2$), the energy gap of frontier orbital ΔEg ($\Delta Eg = E_{LUMO} - E_{HOMO}$) [22,23], the hardness η ($\eta = E_{LUMO} - E_{HOMO}$), the softness σ ($0.5/\eta$) [24,25], the fraction of electrons transferred ΔN from the MD to the bulk iron surface (1 1 0) ($\Delta N = 0.5((\chi_{Fe(110)} - \chi)(\eta_{Fe(110)} + \eta)^{-1})$) [26], where the values of $\chi_{Fe(110)}$ and $\eta_{Fe(110)}$ are 7 and 0 eV mol^{-1}, respectively [27]. The back-donation parameter ΔE_{bd} ($-\eta/4$) of MD and MDH+ was also calculated [28]. Therefore, the local reactivity of the studied structures was examined by analyzing the shapes of the HOMO, LUMO and MEPS surfaces as well as by competing for both Parr and Fukui indices [29,30].

Monte Carlo simulations. The most stable adsorption configurations of DM and DMH+ on the Fe (110) surface were attained from the adsorption locator module using Biovia Materials studio 8.0 [31]. For doing so, the Fe (110) plane was firstly built from Fe crystal and optimized using smart minimizer. Then, the plane was expanded to the supercell of 12×9×12. The simulation of the interaction between adsorbent and Fe (110) surface was implemented in a simulation box of 24.82×24.82×40 Å with periodic boundary conditions. The simulation study was conducted in tow environments: firstly, in a vacuum (MD or MDH+ and Fe (110) surface) and secondly, in solution (MD or MDH+, 500 molecules of water and Fe (110) surface) using COMPASS (condensed-phase optimized molecular potentials for atomistic simulation studies) force field [32].

RESULTS AND DISCUSSION

Corrosion and Adsorption Behavior of MD on Carbon Steel Surface in 1 M HCl

Weight loss analysis, kinetic and thermodynamic parameters. Effect of MD concentration and temperature media: This part aimed to study the influence of MD concentration and temperature media on the progress of corrosion rate of carbon steel (CS) and the inhibition efficiency associated to the MD in corrosive media (1 M HCl) at range temperature of 298-328 K without and with different concentrations of inhibitor (MD), the results are depicted in Table 2. Based on the results in Table 2, the MD has an inhibiting behavior to limit corrosion on CS surface; furthermore, it is observed that the corrosion rate of CS decreases when the concentration of inhibitor increases and consequently the inhibition efficiency of MD increases for the concentration of 5.58 mM; reaching a high value of *IE%* varies from 92% at 298 K to 97% at 328 K. This is probably due to the increase of the surface coverage θ for the studied adsorption; thus, it could be ensured the apparition of the defensive deposit which limits the dissolution of the carbon steel. In other words, it is observed that the inhibition efficiency of MD is slightly increased when the temperature media increases, which probably results in the chemisorption behavior of MD onto CS surface.

Kinetic and thermodynamic parameters of adsorption: According to the Arrhenius plot (Fig. 2) (representation of $\ln(W/T)$ *vs*. 1/T), we calculated the enthalpy $\Delta H°_a$ and entropy $\Delta S°_a$ energies, then the standard activation $E°_a$ was calculated from the plot of $\ln(W)$ against 1/T. These parameters were applied for the carbon steel without inhibitor MD (1 M HCl alone) and with inhibitor (1 M HCl + 5.58 mM of MD) based on the following equations: (Eq. (7)) for $\Delta H°_a$ and $\Delta S°_a$ energies [33] and Eq. (8) for $E°_a$ energy [34]. The output parameters from the Arrhenius

Table 2. The Corrosion Rate of CS (*W*), the Inhibitory Efficiency (*IE%*), and Coverage Surface (θ) in Corrosive Media 1 M HCl at Different Temperatures without and with the Various Concentrations of MD (*C*) Explored from WL Measurements

	C (mM)	*W* (mg cm^{-2} h^{-1})	*IE* (%)
298 °K	1 M HCl	1.032	-
	0.70	0.186	82
	1.40	0.155	85
	2.79	0.103	90
	5.58	0.083	92
308 °K	1 M HCl	1.803	-
	0.70	0.198	89
	1.40	0.180	90
	2.79	0.126	93
	5.58	0.090	95
318 °K	1 M HCl	3.483	-
	0.70	0.348	90
	1.40	0.313	91
	2.79	0.209	94
	5,58	0.139	96
328 °K	1 M HCl	5.883	-
	0.70	0.529	91
	1.40	0.471	92
	2.79	0.235	96
	5.58	0.176	97

plot (Fig. 2) are listed in Table 3,

$$\ln\left[\frac{W}{T}\right] = \ln\left[\left(\frac{R}{N_a h}\right) + \frac{\Delta S_a^\circ}{R}\right] + \left[-\frac{\Delta H_a^\circ}{RT}\right] \quad (7)$$

$$\ln W = \ln A' + \left[-\frac{E_a^\circ}{RT}\right] \quad (8)$$

where *W*, R, T, h and N_a signify the corrosion rate, the

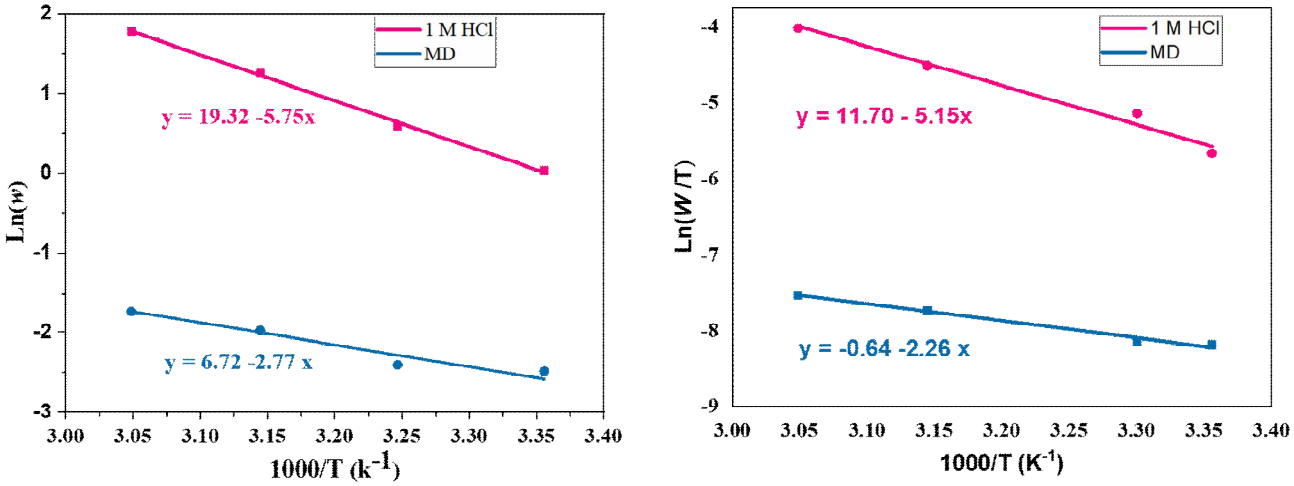

Fig. 2. CS Arrhenius plots in 1 M HCl without and with MD inhibitor (5.58 mM) under different temperatures.

Table 3. Enthalpy ΔH_a° and Entropy $\Delta S°$ Energies for Carbon Steel without MD (1 M HCl Alone) and with MD (1 M HCl + 5.58 mM of MD)

	ΔH_a° (kJ mol^{-1})	ΔS_a° (J mol^{-1} K^{-1})	E_a° (kJ mol^{-1})
1 M HCl	42.85	-100	47.84
MD (5.58 mM)	18.80	-203	23.00

universal constant of the ideal gas, the absolute temperature, the Plank constant, and universal Avogadro number, respectively.

From Table 3, we perceived that the activation standard energy attained in 1 M HCl with MD inhibitor is lower when compared with the blank value. This reflects the chemisorption of adsorption [35]. This character of adsorption can be attributed to the electrons transfer from MD towards empty d-orbitals of iron atoms (main compound of carbon steel) to form both dative and covalent bonds. Moreover, the positive value of standard activation enthalpy reveals the endothermic process of the corrosion phenomenon of carbon steel [36]. In other words, the entropy of activation values is significantly negative for the inhibited solutions compared to that for the uninhibited solutions. This suggests that a rise in randomness happened when moving from reactants to the activated complex [37].

Adsorption isotherm: To gain insight into the adsorption mechanism and the surface behavior of inhibitor molecules, different models of adsorption isotherms were considered. In this current study, the corresponding adsorption with different concentrations of inhibitor under media temperature of 298 °K was tested according to the following isotherms: Langmuir, Temkin, and Frumkin. The results found show that the studied adsorption obeys a Langmuir adsorption isotherm (Fig. 3) assumed by Eq. (9) [38]. As mentioned in Table 4, the linear regression factor of this isotherm model appears to be close to 1,

$$\frac{C}{\theta} = \frac{1}{K_{ads}} + C \qquad (9)$$

where K_{ads} is adsorption coefficient. The K_{ads} values can be

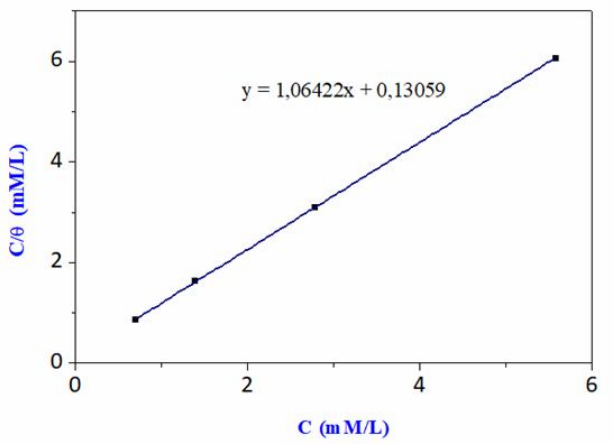

Fig. 3. Langmuir isotherm adsorption model of MD on the carbon steel surface in 1 M HCl at 298 °K.

Table 4. Langmuir Isotherm Adsorption Parameters for 1 M HCl/MD/Carbon Steel Interface at 298 °K

.	K_{ads} (M^{-1})	R^2	ΔG° (kJ mol^{-1})
MD (5.58 mM)	7610.10	0.99	-32.13

calculated from the intercept lines on the C_{inh}/θ axis. The $_{ads}$ is linked to the standard free energy of adsorption ΔG° as follows (Eq. (10)):

$$\Delta G° = - RTln(55.55K_{ads}) \quad (10)$$

The Langmuir isotherm adsorption reflects clearly that the adsorbed molecules of MD occupy only one protective film and that there are no interactions between MD molecules during adsorption [39]. Therefore, it is observed that the value of ΔG° (-32.13 kJ mol^{-1}) is lower -40 kJ mol^{-1} in a negative value. This result suggests that the this adsorption is chemisorption in nature [40].

Electrochemical measurements (EIS and PDP). EIS investigation: The EIS curves of the carbon steel in 1 M HCl were obtained in both the absence and presence of various concentrations of MD after an exposure time of 30 min at 308 K (see Fig. 4). As can be seen in Fig. 4, the increase of MD concentration leads to the increase of the semi-circle diameters of carbon steel, suggesting the prominent role of MD to block corrosion over carbon steel metal. Therefore, the existence of a single semi-circle can be attributed to the presence of a single charge transfer process of adsorption which is not affected by the presence of MD molecules [41]. Otherwise, it is observed that the charge transfer behavior of adsorption is not changed by the addition of MD, and the corrosion inhibition is more probable governed by the charge transfer process [42]. Moreover, the double-layer capacity values *Cdl* calculated in with MD are lower concerning those in the blank solution (HCl alone). This suggests the formation of the protective film during adsorption by MD molecules onto carbon steel surface [43]. The EIS parameters are listed in Table 5. From this table, we noticed that the charge transfer resistance value *Rct* increases with the increase of MD concentration leading to a high value of 761.4 Ω cm^2 with inhibitory efficiency of 97% at 5.60 mM. Thus, it reveals that MD molecules can be considered as a useful inhibitor to protect

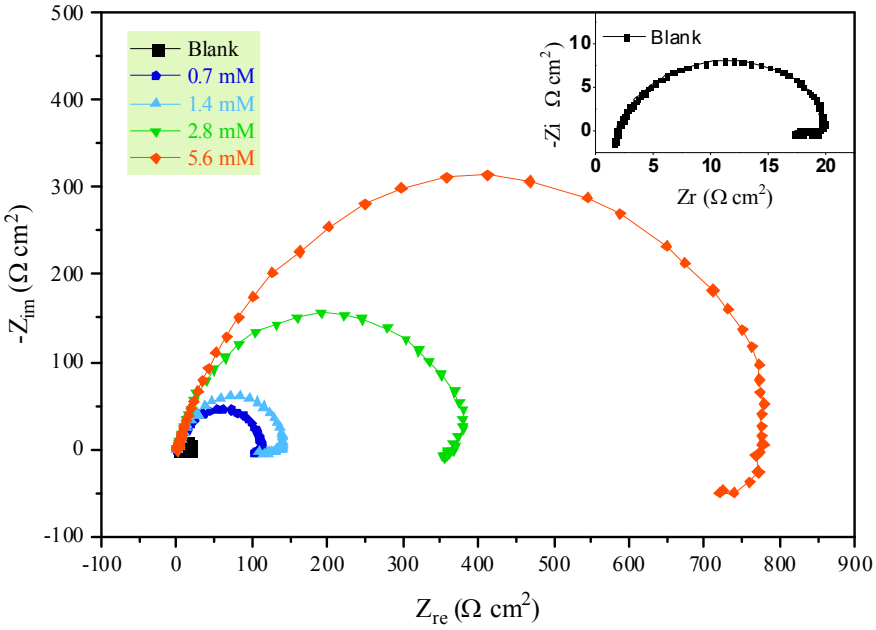

Fig. 4. Nyquist plots for carbon steel in 1 M HCl without and with different concentrations of MD at 308 °K.

Table 5. EIS Parameters for Carbon Steel in 1 M HCl without and with Different Concentrations of MD at 308 °K

Inhibitor		R_{ct} (Ω cm²)	R_s (Ω cm²)	C_{dl} (μF cm⁻²)	*IE* (%)
Blank (1 M)	1.0	16.96	2 .149	84.12	-
MD (mM)	0.7	108.8	2.475	73.17	84
	1.4	132.4	3.727	60	87
	2.8	361.1	3.911	55	95
	5.6	761.4	5.939	52	97

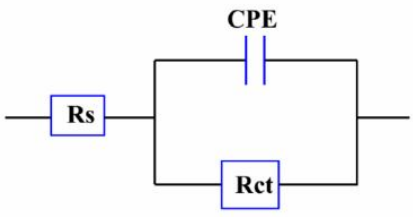

Fig. 5. The equivalent circuit used to fit the electrochemical impedance spectroscopy (EIS) data.

carbon steel against corrosion and to reduce the reactive sites which could be created during the corrosion phenomenon.

PDP investigation: Potentiodynamic polarization curves (anodic and cathodic) of carbon steel in 1 M HCl were obtained without and with different concentrations of MD (Fig. 6). Then, the output parameters of PDP analysis are given in Table 6. From Fig. 6, we noticed that both cathodic and anodic curves were translated to lower current densities with an increase of MD concentration. Furthermore, the corresponding corrosion potential was appeared approximately constant, signifying that MD into adsorption acts as a mixed type inhibitor [44]. Additionally, we noticed that the current density values of corrosion are decreased with an increase of MD concentration leading to a minimum value of 26 $\mu A\ cm^{-2}$ with inhibitory efficiency of 89% at 5.60 mM. This result suggests that MD can be considered as a good inhibitor to limit the deterioration of carbon steel in the acidic medium of HCl.

Computational Inquiries Using DFT, MESP and MC Approaches

DFT, MESP and MC calculations were performed to clarify the affinity of MD molecules to adsorb and form protective layers onto the iron surface.

DFT and MESP calculations: DFT and MESP calculations were conducted to describe physico-chemical properties of both neutral forms of MD and its protonated form MDH+. The optimized structures, the frontier orbital (HOMO and LUMO) shapes, and MESP maps are exposed in Fig. 7. Global DFT parameters of MD and MDH+ such as EHOMO, ELUMO, the energy gap of frontier orbital ΔEg, the electronegativity χ, the hardness η, the softness σ, the fraction of electrons (ΔN) transferred from the MD or MDH+ to the bulk iron surface (110) and the back-donation character (ΔE_{bd}) were calculated. These parameters are obtained based on the relationships described in section 2.4.1 of the manuscript. These parameters are gathered in Table 7.

According to Fig. 7, we noticed that protonation of MD does not provide a change at the level of LUMO distribution, while for HOMO, it is observed that the protonation of MD causes an appearance of new areas of HOMO. This result indicates that the protonated form of MD (MDH+) has a higher tendency to donate electrons to empty 3d orbital of iron atoms available on the studied surface compared to the neutral form of MD, which is confirmed by the higher electronegativity of the MDH+ (8.98 eV) compared to the MD (3.34 eV). It could lead to the increase of reactivity and adsorption of MD onto the iron surface. On the other hand, it is noticed that both HOMO and LUMO are very concentrated at oxazole ring of MD and MDH+, suggesting the prominent role of oxazole group to reach more adsorption of these compounds onto the iron surface. From MEPS maps we looked that forte negative charge density (Forte NCD) which is defined by the red color region strongly localized on the oxazole ring of MD, while for MDH+, we noticed that the oxazole group represents this forte positive charge density (Forte PCD) that is defined as a blue region. Based on the results, it must be concluded that the oxazole ring is very important to assure donating and accepting electrons behaviors during the studied adsorption and consequently, the inhibitory efficiency because of the adsorption of the inhibitory compounds MD and MDH+.

From Table 7, we noticed that the value of ΔN in the case of MD (0.29 e) is positive and less than 3.6 e, suggesting the high ability of MD molecules to donate electrons to vacant d orbitals of iron on the surface. In contrast, the negative value of ΔN for MDH+ (-0.19 e) indicates that MDH+ species have a high capability to accept electrons of metal. Therefore, comparing ΔE_g and ΔE_{bd} of MD with those of MDH+ shows that MDH+ is associated with a lower values of ΔE_g and ΔE_{bd}, suggesting that accepting electrons in MDH+ species is more preferred than donating electrons in MD species.

Both Fukui functions (f- and f+) and Parr functions (P- and P+) are used to understand the reactive sites of the MD inhibitor responsible for the nucleophilic and electrophilic reaction attacks. The values corresponding to the Fukui and Parr functions are listed in Table 8 as follows: f- and P- for an electrophilic attack on MD and f+ and P+ for a nucleophilic attack on MD.

According to Table 8, the maximum values of f+ and P+ are located on C (1), C (2), O (27), N (28) and C (29). However, the maximum values of f- and P- are situated on C (1) and N (28). This result indicates that the nucleophilic attacks from the iron surface on MD molecules are more

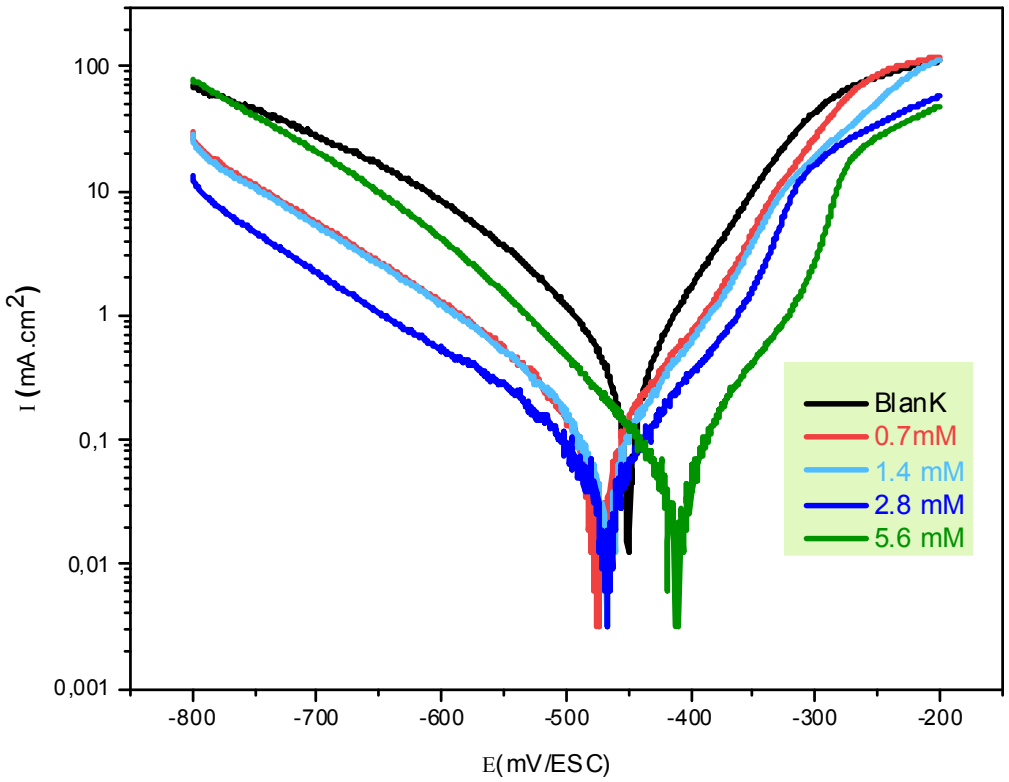

Fig. 6. Anodic and cathodic polarization curves of mild steel in solutions of 1 M HCl without and with different concentrations of MD.

Table 6. Electrochemical Parameters for Carbon Steel at Different Concentrations of MD Studied in 1 M HCl at 308 K

Inhibitor		-Ecorr (mv/ESC)	i_{corr} ($\mu A\ cm^{-2}$)	Tafel slopes (mv dec^{-1})		*EI* (%)
				β_a	$-\beta_c$	
Blank (M)	1 M	450.0	420	71.9	105.2	
MD (mM)	0.7	475.5	236	83.6	166.5	44.0
	1.4	412.0	111	64.4	120.2	73.5
	2.8	467.9	67.5	94.2	153.3	84.0
	5.6	410	26.0	53.6	46.7	89.0

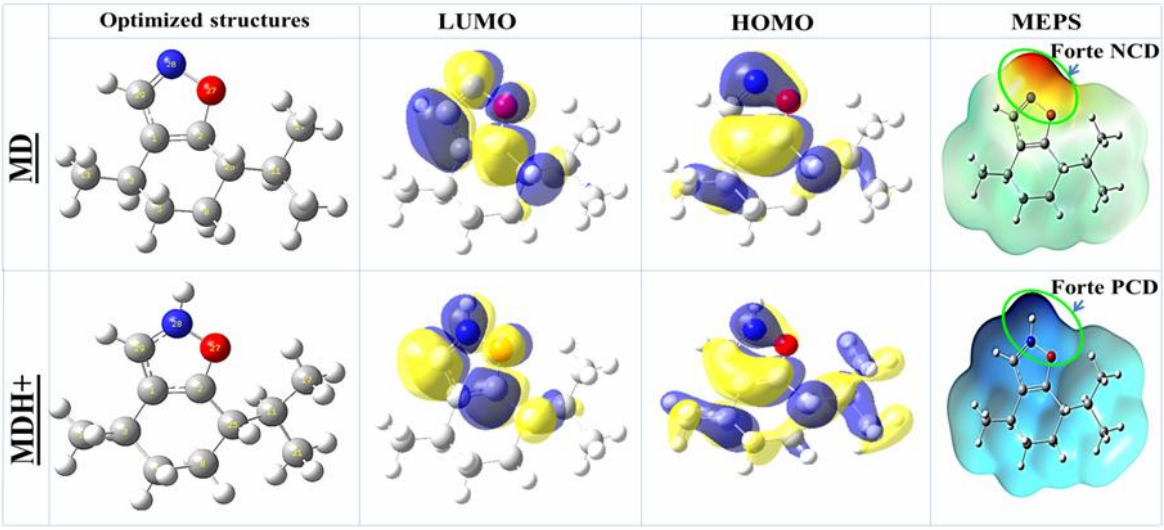

Fig. 7. Optimized structures, LUMO, HOMO orbital, and MEPS maps of MD and MDH+. Note for MESP: forte NCD (*i.e*., forte negative density charge) and forte PCD (*i.e,* forte positive density charge).

Table 7. Global Quantum Parameters in eV (Expect ΔN in e**)** of MD and MDH+

	E_{HOMO}	E_{LUMO}	ΔEg	χ	η	σ	ΔN	ΔE_{bd}
MD	-6.53	-0.15	6.38	3.34	6.38	0.08	0.29	-1.60
MDH+	-11.70	-6.25	5.45	8.98	5.45	0.09	-0.19	-1.36

important than the electrophilic attacks of MD molecules on the iron surface. Furthermore, it must be noticed that all reactive sites are localized throughout the oxazole ring of MD, which is in agreement with the electron acceptor character of the MD molecules during adsorption. We concluded from the above results that the adsorption regions of MD and/or MDH+ on Fe (110) include unsaturated double bonds C=C, C=N, C=NH+, sp2 nitrogen atom (>N=) and/or sp3 oxygen atom (-O-) of oxazole group.

Monte Carlo simulations: In the context of the Monte Carlo calculations, adsorption energy (E_{ads}) is a very important parameter which represents a direct tool to classify the efficiency of the studied inhibitors. This energy is defined according to the following equation (Eq. (11)) [40].

$$E_{adsorption} = E_{total} + E_{solution} - (E_{surface+solution} + E_{inhibitor+solution}) \quad (11)$$

where E_{total}, $E_{surface+solution}$, $E_{inhibitor+solution}$, and $E_{solution}$ correspond respectively to the total energy of interface (substrate/adsorbent), the total energy of the surface and solution, the total energy of the system except the iron surface, and the total energy of the solution.

Briefly, the adsorption energy is defined as the sum of both the rigid adsorption energy (E_{Rads}) and the deformation energy (E_{Def}). Another term of energy, noted dEads/dNinhibitor, represents the amount of energy required to remove one entity of inhibitor to the iron surface (110). These energies are calculated in the solution medium of ($460H_2O$, $20H_3O^+$ and $20Cl^-$) and reported in Table 9.

Table 8. Calculated Values of Fukui and Parr's Functions Associated with the Significant Atoms of MD

	Fukui functions *f*-/ *f*+		Parr functions *P*-/*P*+	
Atoms	*f*-	*f*+	*P*-	*P*+
C (1)	0.22283	0.25952	0.400641	0.451610
C (2)	0.18994	0.19696	0.023893	0.166019
C (3)	-0.03359	-0.01801	-0.057834	0.040936
C (5)	-0.01431	-0.01140	0.021347	0.020946
C (8)	-0.01505	-0.01278	0.020958	-0.022811
C (11)	0.00130	-0.00293	0.037077	-0.014727
C (13)	-0.01015	-0.01329	-0.022413	0.020089
C (17)	-0.00759	-0.00789	-0.010893	0.001674
C (21)	-0.00531	-0.00766	0.012188	-0.012346
C (25)	-0.02562	-0.02171	0.010394	0.014347
O (27)	0.02222	0.69185	-0.180420	0.753447
N (28)	0.19675	0.17720	0.483541	0.195935
C (29)	-0.00451	0.12177	-0.203250	0.139806

Table 9. Calculated Energies (in kcal mol^{-1}) by the Mont Carlo Simulation for the Lowest Adsorption Configurations of Inhibitor (MD or MDH+) on the Iron Surface (110) in the Solution Medium ($460H_2O$, $20H_3O^+$, $20Cl^-$)

Inhibitor	E_T	E_{ads}	E_{Rads}	E_{Def}	$dE_{ads}/dN_{inhibitor}$
MD	-9448.97	-9452.01	-9799.93	347.91	-110.44
MDH+	-9528.20	-9487.60	-9815.22	327.62	-130.06

Top and side views of the more stable configurations of MD and MDH+ are shown in Fig. 9. From this figure, it is observed that both MD and MDH+ are adsorbed almost on flat orientations onto the iron surface (110) to maximize the surface coverage and contact.

Table 9 shows that MDH+/solution/Fe (110) interface is more stable (has low value of E_T) than MD/solution /Fe (110). Further, the negative values of E_{ads} suggest that the studied adsorption is spontaneously shaped [45]. Moreover, it is noticed that MDH+/solution/ Fe (110) interface has a highest negative value of E_{ads} (-9487.60 mol^{-1}) compared to the MD/solution/Fe (110) interface (-9452.01 mol^{-1}), indicating a stronger interaction between the MDH+ and the iron surface (110) in the acidic

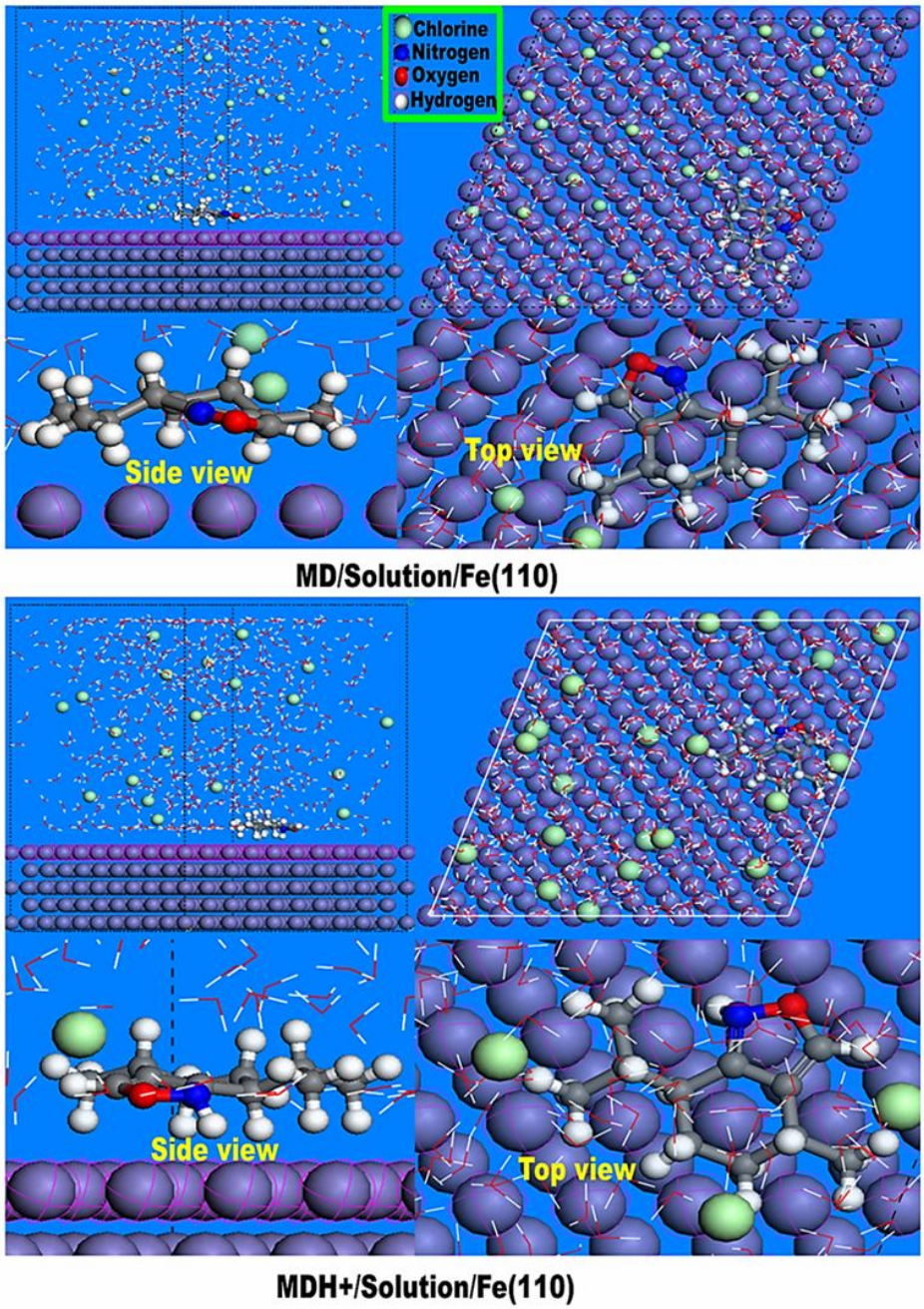

Fig. 9. Top and side views of stable adsorption configurations of MD and MDH+ inhibitors on Fe surface in solution ($460H_2O$, $20H_3O^+$ and $20Cl^-$).

solution; this is proposing that the protonation process of MD molecules has been severed to the high reactivity of MD towards the iron surface.

CONCLUSIONS

In this study, the inhibition corrosion behavior of MD

on carbon steel surface was explored using experimental inquiries (WL, EIS and PDP). The DFT calculation, MESP and MC simulations were additionally used to explain the anti-corrosion mechanism of the inhibitor. Based on the data analysis related to the WL measurements, the increase of MD concentration leads to the increase of the inhibitory efficiency reaching up about 97% at 5.58 mM and 308 °K. Then, the inhibition ability of MD is better than that of menthone (90% at 6.48 mM at 298 K) in the same condition. Effectively, the MD has an oxazole group with a high tendency to coordinate with metals, which provides it with the high anticorrosive property for carbon steel. The adsorption of MD on the carbon steel surface follows a Langmuir adsorption isotherm, suggesting that there is no any interaction between the adsorbed molecules of MD, MDH+ and molecules of one protective layer over the metal surface. According to PDP analysis data, we demonstrated that the corrosion inhibitory is the mixed type. Furthermore, the computation of both activation standard energy ($E°_a$) and activation Gibbs free energy ($\Delta G°$) indicates that the adsorption is chemisorption in nature. The theoretical findings showed a good agreement with the results of different experimental techniques. For the future study, we are interested in evaluating the corrosion inhibition effect of the MD compound on the other metal surfaces and in another aggressive medium either acidic, neutral, or basic.

ACKNOWLEDGEMENTS

We would like to thank the Moroccan Association of theoretical chemists (AMCT) for access to the computational facility.

Conflict of Interest

No conflicts to declare.

REFERENCES

[1] A.K. Singh, A.K. Pandey, P. Banerjee, S.K. Saha, B. Chugh, S. Thakur, B. Pani, P. Chaubey, G. Singh, J. Environ. Chem. Eng. 7 (2019) 102971.

[2] A.K. Singh, S. Thakur, B. Pani, B. Chugh, H. Lgaz, I.-M. Chung, P. Chaubey, A.K. Pandey, J. Singh, J. Mol. Liq. 283 (2019) 788.

[3] M.Y. El Sayed, A.M. Abdel-Gaber, H.T. Rahal, J. Fail. Anal. Prev. 19 (2019) 1174.

[4] G.A. Swetha, H.P. Sachin, A.M. Guruprasad, B.M. Prasanna, J. Fail. Anal. Prev. 19 (2019) 1113.

[5] L.R. Chauhan, G. Gunasekaran, Corros. Sci. 49 (2007) 1143.

[6] S. Kharchouf, L. Majidi, M. Znini, J. Costa, B. Hammouti, J. Paolini, Int. J. Electrochem. Sci. 7 (2012) 10325.

[7] Z. Faska, A. Bellioua, M. Bouklah, L. Majidi, R. Fihi, A. Bouyanzer, B. Hammouti, Monatshefte Für. Chem.-Chem. Mon. 139 (2008) 1417.

[8] Z. Faska, L. Majidi, R. Fihi, A. Bouyanzer, B. Hammouti, Pigment Resin Technol. (2007).

[9] S. Kharchouf, L. Majidi, M. Bouklah, B. Hammouti, A. Bouyanzer, A. Aouniti, Arab. J. Chem. 7 (2014) 680.

[10] A. Ansari, M. Znini, I. Hamdani, L. Majidi, A. Bouyanzer, B. Hammouti, J. Mater. Env. Sci. 5 (2014) 81.

[11] C. Verma, L.O. Olasunkanmi, I.B. Obot, E.E. Ebenso, M.A. Quraishi, RSC Adv. 6 (2016) 53933.

[12] C. Verma, H. Lgaz, D.K. Verma, E.E. Ebenso, I. Bahadur, M.A. Quraishi, J. Mol. Liq. 260 (2018) 99.

[13] A. Ansari, A. Oubair, M. Znini, Int. J. Innov. Appl. Stud. 24 (2018) 1819.

[14] G. ASTM, G 1-03, Standard Practice for Preparing, Cleaning, and Evaluating Corrosion Test Specimens," Philadelphia, Pennsylvania: American Society for Testing and Materials, 2003.

[15] R. Nabah, F. Benhiba, Y. Ramli, M. Ouakki, M. Cherkaoui, H. Oudda, I. Warad, A. Zarrouk, Anal. Bioanal. Electrochem. 10 (2018) 1375.

[16] M. Znini, A. Ansari, J. Costa, O. Senhaji, J. Paolini, L. Majidi, Anal. Bioanal. Electrochem. 11 (2019) 1426.

[17] J. Tan, L. Guo, D. Wu, R. Yu, F. Zhang, S. Kaya, Int. J. Electrochem. Sci. 15 (2020) 1893.

[18] C. Verma, L.O. Olasunkanmi, I.B. Obot, E.E. Ebenso, M.A. Quraishi, RSC Advances 6 (2016) 53933.

[19] M.J. Frisch, G.W. Trucks, H.B. Schlegel, G.E. Scuseria, M.A. Robb, J.R. Cheeseman, G. Scalmani, V. Barone, B. Mennucci, G.A. Petersson, Gaussian 09 Revision D. 01, 2009, Gaussian Inc, Wallingford CT. 93 (2009).

[20] W.J. Hehre, R. Ditchfield, J.A. Pople, J. Chem. Phys. 56 (1972) 2257.
[21] P.C. Hariharan, J.A. Pople, Theoretica Chimica Acta 28 (1973) 213.
[22] R. Hssissou, B. Benzidia, N. Hajjaji, A. Elharfi, Elaboration, Portugaliae Electrochimica Acta 37 (2019) 179.
[23] P. Geerlings, F. De Proft, W. Langenaeker, Chem. Rev. 103 (2003) 1793.
[24] K. Vanasundari, V. Balachandran, M. Kavimani, B. Narayana, J. Mol. Struct. 1147 (2017) 136.
[25] A. Benallou, Z. Lakbaibi, H. Garmes, H.E.A. El Abdallaoui, J. Fluorine Chem. 219 (2019) 79.
[26] S. Martinez, Mater. Chem. Phys. 77 (2003) 97.
[27] A. Kokalj, Chem. Phys. 393 (2012) 1.
[28] L.O. Olasunkanmi, M.M. Kabanda, E.E. Ebenso, Physica E: Low-Dimensional Systems and Anostructures 76 (2016) 109.
[29] C.M. Goulart, A. Esteves-Souza, C.A. Martinez-Huitle, C.J.F. Rodrigues, M.A.M. Maciel, A. Echevarria, Corrosion Sci. 67 (2013) 281.
[30] L.R. Domingo, P. Pérez, J.A. Sáez, RSC Adv. 3 (2013) 1486.
[31] H. Sun, J. Phys. Chem. B 102 (1998) 7338.
[32] S. Martinez, I. Stern, Appl. Surface Sci. 199 (2002) 83.
[33] O. Benali, O. Cherkaoui, A. Lallam, J. Mater. Environ. Sci. 6 (2015) 598.
[34] A.M. Badiea, K.N. Mohana, Corrosion Sci. 51 (2009) 2231.
[35] S. Kharchouf, L. Majidi, M. Znini, J. Costa, B. Hammouti, J. Paolini, Int. J. Electrochem. Sci. 7 (2012) 10325.
[36] R. Hsissou, F. Benhiba, S. Abbout, O. Dagdag, S. Benkhaya, A. Berisha, H. Erramli, A. Elharfi, Inorg. Chem. Commun. (2020) 107858.
[37] M. Alfakeer, M. Abdallah, A. Fawzy, Int. J. Electrochem. Sci. 15 (2020) 3283.
[38] Y. Kharbach, F.Z. Qachchachi, A. Haoudi, M. Tourabi, A. Zarrouk, C. Jama, L.O. Olasunkanmi, E.E. Ebenso, F. Bentiss, J. Mol. Liq. 246 (2017) 302
[39] A.H. Tantawy, K.A. Soliman, H.M. Abd El-Lateef, Journal of Cleaner Production 250 (2020) 119510.
[40] A. Abdeslam, M. Mounir, Z. Mohamed, L. Zouhair, A. Mohamed, Mediterranean J. Chem. 10 (2020) 62.
[41] N. Errahmany, M. Rbaa, A.S. Abousalem, A. Tazouti, M. Galai, E.H.E. Kafssaoui, M.E. Touhami, B. Lakhrissi, R. Touir, J. Mol. Liq. (2020) 113413.
[42] R. Padash, G.S. Sajadi, A.H. Jafari, E. Jamalizadeh, A.S. Rad, Mater. Chem. Phys. 244 (2020) 122681.
[43] M. Rbaa, P. Dohare, A. Berisha, O. Dagdag, L. Lakhrissi, M. Galai, B. Lakhrissi, M.E. Touhami, I. Warad, A. Zarrouk, Journal of Alloys and Compounds (2020) 154949.
[44] E.E. Ebenso, M.M. Kabanda, L.C. Murulana, A.K. Singh, S.K. Shukla, Indust. Engin. Chem. Res. 51 (2012) 12940.
[45] M. Manssouri, A. Laghchimi, A. Ansari, M. Znini, Z. Lakbaibi, Y. El Ouadi, L. Majidi, Mediterranean J. Chem. 10 (2020) 253.